

Defining and controlling double quantum dots in single-walled carbon nanotubes

M R Gräber, M Weiss, S Oberholzer and C Schönenberger

Institut für Physik, Universität Basel, Klingelbergstrasse 82, CH-4056 Basel, Switzerland

E-mail: christian.schoenenberger@unibas.ch

Received 9 May 2006

Published 17 October 2006

Online at stacks.iop.org/SST/21/S64

Abstract

We report the experimental realization of double quantum dots in single-walled carbon nanotubes. The device consists of a nanotube with source and drain contact, and three additional top-gate electrodes in between. We show that, by energizing these top gates, it is possible to locally gate a nanotube, to create a barrier, or to tune the chemical potential of a part of the nanotube. At low temperatures, we find (for three different devices) that in certain ranges of top-gate voltages our device acts as a double quantum dot, evidenced by the typical honeycomb charge stability pattern.

(Some figures in this article are in colour only in the electronic version)

1. Introduction

Since their discovery in 1991 [1] carbon nanotubes have, due to their unique mechanical and electronic properties, been the subject of tremendous scientific and technological interest. In the field of mesoscopic physics, carbon nanotubes offer an easily accessible experimental platform for studying the physics of the textbook example of a particle trapped inside a box, a so-called quantum dot or artificial atom [2, 3]. Single quantum dots can simply be realized by contacting a nanotube with two metallic contacts (normally made of palladium); the contacts between the nanotube and the metallic leads usually act as tunnel barriers, characterized by the nanotube–lead tunnelling rate Γ and a capacitance C . The energy scales for nanotube quantum dots are given by a typical single-electron charging energy $U_C \approx 3 \text{ meV} \approx 30 \text{ K}$ and a quantum-mechanical level spacing $\delta E = \frac{h v_F}{2L}$, where h is Planck's constant. Using the Fermi velocity $v_F = 8 \times 10^5 \text{ m s}^{-1}$ and an effective nanotube length $L = 1 \text{ }\mu\text{m}$ the level spacing amounts to $\delta E \approx 2 \text{ meV}$.

However, the standard approach for manufacturing quantum dot devices has relied on structures in GaAs-based two-dimensional electron gases (2-DEG), which can be defined using etching and gating techniques. The main advantage of this system is the high degree of control over the quantum dot properties, which has been achieved over the last few years. These quantum dots allow for a precise tuning of the coupling to the leads by energizing locally

acting gate electrodes, see e.g. [4] and references therein. Additionally, centre gates can be used in order to define double quantum dot structures with a tunable inter-dot coupling. This tunability is an essential ingredient for further experiments exploring the nature of electronic states in quantum dots or, even more ambitious, for realizing quantum electronic devices such as spin- or charge-based quantum bits [5–7]. As this high degree of control has been lacking in nanotube-based quantum dots so far, using carbon nanotubes offers fascinating opportunities. For example, new physical phenomena such as superconducting correlations or spin injection into quantum dots can be studied in carbon nanotube quantum dots [8, 9]. In contrast to carbon nanotubes, up to now it has not been possible to attach ferromagnetic and superconducting to GaAs-based quantum dots. Moreover, the influence of the surrounding nuclear spins is expected to limit electron spin dephasing times in GaAs (double) quantum dots [10]. In carbon nanotubes, on the other hand, nuclear spins are predominantly absent and hyperfine interactions thus strongly reduced. The question to what degree carbon nanotube quantum dots can be tuned using locally acting gate electrodes is therefore an important issue to address. In this paper, we describe a technique of implementing local top-gate electrodes onto a single-walled carbon nanotube (SWNT). After characterizing the functionality of the top gates, we will then make use of them in order to define and control the double quantum dots inside SWNTs.

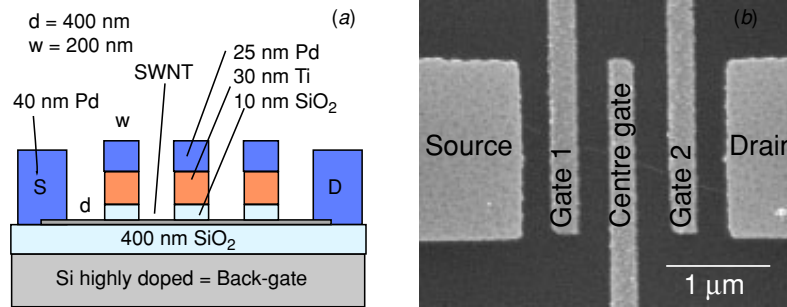


Figure 1. (a) Side-view schematic of a SWNT device with three top gates. (b) Scanning electron micrograph of the device. Gates are labelled gate 1, centre gate and gate 2 (from source to drain).

2. Local gating of carbon nanotubes

2.1. Strategies for gating nanotube quantum dots

With the nanotube lying on an oxidized Si substrate, a natural way of gating this single quantum dot is to apply a voltage to the doped Si substrate. The Si then acts as a back gate globally affecting the whole quantum dot. In order to create multiple dots in such a device and control them independently, however, one will need to find a way of locally gating a nanotube. By using such local gates, one can either create a barrier or simply shift the chemical potential within a small part of the nanotube. In the following, we will briefly review two different strategies of local gating of nanotubes that have been reported in the literature, and will describe in detail the technique that has been developed in our lab. At the end of this section, the measurements of electrical transport through nanotube devices with local gates are presented.

In order to fabricate gate electrodes locally acting on a nanotube, side gates represent a straightforward option [11]. Besides source and drain contacts, additional electrodes are patterned in the vicinity of the nanotube. The advantage of this technique is that contacts and side gates can be fabricated within the same processing step. It is, however, difficult to get the side gates as close to the nanotube as possible, yet not contacting it electrically. Thus, typically side gates are spaced by approximately 100 nm from the SWNT, making the gating less efficient and their action less local.

More efficient are the gates made by directly evaporating the gate electrode on top of the nanotube, with a thin gate oxide underneath. These so-called top gates are spaced from the SWNT only by the thickness of the gate oxide ($\approx 1\text{--}10$ nm), making them act more efficiently and (depending on their width) more locally as compared to the side gates. Despite the fact that there are drawbacks of this method as well (additional processing steps, nanotube properties may be modified underneath the top gates), top gates are the most promising approach for creating local barriers in the SWNT. Therefore, we have developed a reliable method for fabricating top-gate electrodes in our laboratory, which we will now discuss in more detail.

2.2. Experimental details

SWNTs were grown on a degenerately doped Si/SiO₂ substrate by means of chemical vapour deposition (CVD).

The details of the CVD process can be found elsewhere [12]. After the initial preparation of SiO₂/Ti/Au bond pads and alignment markers, SWNTs were then located with a scanning electron microscope (SEM). In the following step, the gate electrodes were defined by e-beam lithography. Electron-gun evaporation of SiO₂ as gate oxide, Ti as gate metal and Pd serving as an anti-oxidation cover layer followed. The gate-oxide film thickness was chosen to be 10 nm, the Ti film thickness 30 nm and that of the Pd layer 25 nm. The materials were evaporated at a pressure of $\approx 10^{-7}$ mbar. In a final lithography and evaporation step, the source and drain electrodes of the nanotube, consisting of 40 nm Pd, were defined. The evaporation conditions were the same as described above, except that the substrate was kept at a constant temperature of ≈ 0 °C by cooling the sample holder inside the evaporation chamber. This cooling helps to reduce outgassing of materials inside the vacuum chamber due to heating during the evaporation. After lift-off of the remaining polymethyl methacrylate (PMMA), the samples were glued into a 20-lead chip carrier and bonded. Figures 1(a) and (b) show a side-view schematic and a scanning electron micrograph of a typical SWNT device with the three top gates in addition to the source and drain electrodes. The spacing between the source and drain electrodes amounts to 2.2 μm , and the width of the gates was chosen to be 200 nm. The back-gate oxide has a commonly used thickness of 400 nm.

2.3. Effect of local gate electrodes at 300 K and 4.2 K

In figure 2(a), the linear conductance versus the gate voltage of a device with the three top-gate electrodes is plotted. The gate dependence identifies the semiconducting nature of the SWNT. At a voltage of roughly 0.6 V applied to either of the three top gates, the conductance through the device is suppressed indicating that the chemical potential is shifted locally into the semiconducting gap of the SWNT. After a decrease of conductance for an increasing gate voltage, the conductance increases again for more positive gate voltages. This behaviour is explained by the band diagram sketched in the inset of figure 2(a). Intrinsically, the tube is p-doped and the chemical potential μ resides in the valence band (i). For an increasing voltage at the top gate the potential landscape is changed locally, making μ lie within the energy gap below the gate (ii). In this scenario, the conductance through the nanotube reaches its minimum. With this technique, it should thus be possible to create local barriers inside a carbon nanotube, allowing one

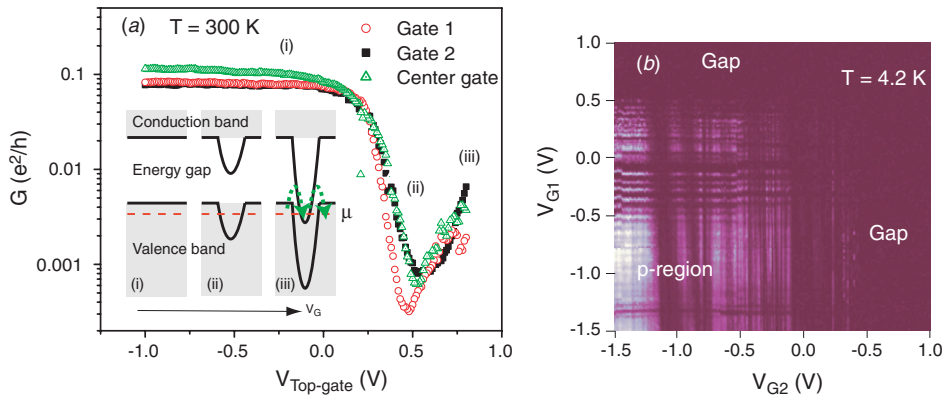


Figure 2. (a) Linear conductance G on a logarithmic scale for a device with three top-gate electrodes (oxide thickness 10 nm) versus top-gate voltage at $T = 300$ K. The non-swept gates are connected to the ground potential. Inset: (i)–(iii) illustrate the band structure for an increasing top-gate voltage. (b) The colour-scale plot (dark = 0, bright = $0.008 e^2 h^{-1}$) of the conductance versus gates 1 and 2 for a constant centre-gate voltage at 4.2 K.

to create artificial potential landscapes. If the gate voltage is increased even more, the lower edge of the conduction band will eventually reach the upper edge of the valence band (iii). Now, thermally activated band-to-band processes indicated by the green arrows are possible and the conductance increases again. We have observed such behaviour only at 300 K indicating the large activation barriers involved in these band-to-band charge transfer processes. Band-to-band charge transfer processes have also been reported in [13].

In figure 2(b) the linear differential conductance at 4.2 K versus voltages applied at the top gates 1 and 2 for a constant centre-gate voltage of $V_C = -1$ V is plotted on a colour scale (bright = more conductive). At voltages of around 0.5 V applied to either of the top gates, the chemical potential is shifted into the energy gap of the nanotube and the electrical transport is suppressed. For lower top-gate voltages, sweeping gate 1 and gate 2 leads to pronounced oscillations of the conductance due to single-electron charging and finite-size effects of the nanotube, which are accessible at low temperatures.

3. Nanotube double quantum dots

3.1. Previous work

Recently, in the field of double quantum dots in carbon nanotubes, an enormous progress has been achieved. In 2004, Mason *et al* first demonstrated the local gate control of an intrinsic double quantum dot inside a carbon nanotube [15]. This work was then extended by the same group in [16], where a tunable mutual capacitance was demonstrated. In a recent work, Sapmaz *et al* could observe electronic transport through excited states as seen in finite-bias triangles in a SWNT double dot [17]. In [18] molecular eigenstates of a strongly coupled carbon nanotube double quantum dot were observed and analysed.

3.2. Experimental data

In this section we will show that it is possible to reliably define clean double quantum dots in SWNTs by using the

top-gate electrodes. We focus on three devices labelled A, B, C with three top gates each. Samples A and B were fabricated according to figure 1(a). In the case of device C, the source–drain spacing was reduced to $1.4 \mu\text{m}$ and the top-gate width to 100 nm. Whereas devices A and B are based on a semiconducting SWNT (operated in the hole regime), device C is metallic. In figures 3(a)–(c), the differential conductance versus voltages applied at two top gates is plotted on a colour scale (bright = more conductive). For devices A and C, the centre gate has been set to a constant value of -0.1 V and 0 V, respectively, and gates 1 and 2 are swept. In the case of device B, the centre gate and gate 1 are swept, while gate 2 was kept at a constant voltage of $V_{G2} = -0.1$ V. The visible high-conductance ridges as observed for all three devices define a charge-stability map that is shaped like a honeycomb. This honeycomb pattern is characteristic of a double quantum dot. Within each cell, the number of holes (n, m) on the two dots is constant. Energizing gate 1 (2) to more negative voltages successively fills the holes into dot 1 (2), whereas a more positive voltage pushes the holes out of the dot. The fact that all three devices can be tuned to exhibit a honeycomb pattern shows that the double quantum dots are indeed defined by the local gates and are not intrinsic to the nanotube. Common to all three devices is that the applied gate voltages are close to 0 V, i.e. far off the pinch-off voltage. In such a regime, we expect a smooth modulation of the electronic potential rather than sharp and steep barriers.

The honeycomb charge stability map allows for a quantitative determination of the double dot capacitances as defined in the electrostatic double dot model in figure 3(e), following the work of van der Wiel *et al* [14]. As an example, we will determine the capacitances of the double dot defined in device C, see figure 3(c). From the dimensions of the honeycomb cell, one can extract the gate capacitances

$$C_{G1/2} = |e|/\Delta V_{G1/2}, \quad (1)$$

yielding $C_{G1} \approx 30$ aF and $C_{G2} \approx 25$ aF. Of particular importance are the points where the three charge states are degenerate, the so-called triple points. Two such points are marked by dashed circles in figure 3(b) for clarity. When applying a finite-bias voltage, the triple points transform into

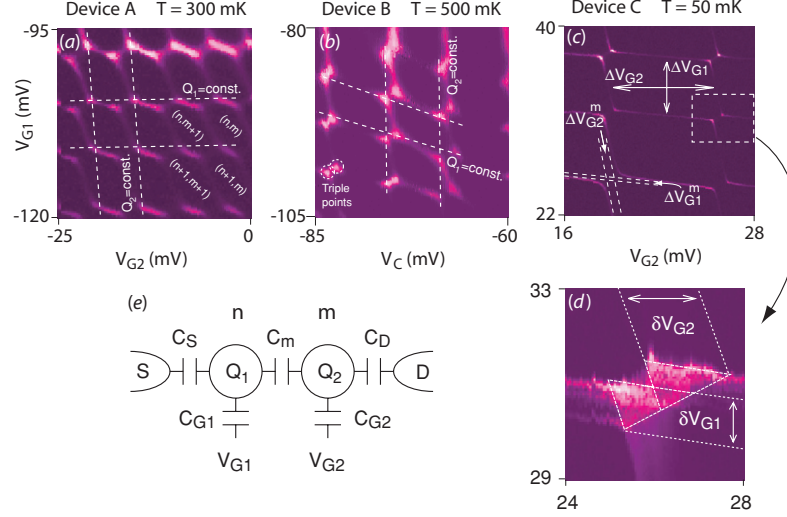


Figure 3. (a) Colour-scale plot of the conductance versus top-gate voltages at 300 mK for device A. Bright corresponds to $0.4 e^2 h^{-1}$. The obtained honeycomb pattern is the charge stability map of a double quantum dot. (b) Same for device B at 500 mK, bright corresponds to $0.08 e^2 h^{-1}$. (c) Same for device C at 50 mK, bright corresponds to $0.035 e^2 h^{-1}$. (d) Zoom into the triple-point region marked by the dashed box in (c) at a bias voltage of $V_{sd} = 500 \mu\text{V}$. (e) The capacitive model of a double quantum dot.

triangles, in which the transport is enabled. Figure 3(d) shows the triple-point region within the dashed box of figure 3(c) at an applied source–drain voltage of $V_{sd} = 500 \mu\text{V}$. From the dimensions of these triangles $\delta V_{G1(G2)}$ and

$$C_{G1(G2)}/C_{1(2)} = |V_{sd}|/\delta V_{G1(G2)}, \quad (2)$$

we obtain the total capacitance $C_1 = C_s + C_{G1} + C_m \approx 60 \text{ aF}$ and $C_2 = C_d + C_{G2} + C_m \approx 75 \text{ aF}$ of dots 1 and 2, respectively. Here, C_m denotes the mutual capacitance and $C_{s(d)}$ the capacitance of the tunnel barrier to the source (drain). In a purely electrostatic model, the mutual capacitance can be evaluated from the spacing of two adjacent triple points. This spacing, however, is influenced by the tunnel coupling t in between the two dots as well. This quantum mechanical effect leads to a level anti-crossing, resulting in curved wings in the vicinity of the triple points. A rough estimate of the mutual capacitance, however, can be achieved by drawing the asymptotes to the curved borders of the honeycomb, see the bottom left triple-point region of figure 3(c). From the vertical (horizontal) distance ΔV_{G1}^m (ΔV_{G2}^m), it is then possible to extract C_m by using

$$\Delta V_{G1,2}^m = |e|C_m/C_{G1,2}C_{2,1}. \quad (3)$$

We obtain a mutual capacitance of $C_m \approx 5 \text{ aF}$. Additionally, analysing the curvature of the honeycomb borders allows one to precisely evaluate the tunnel coupling t . For a detailed description of this we refer to [18], where it was found that t can exceed the electrostatic nearest-neighbour interaction by as much as an order of magnitude. This fact reflects the one-dimensional geometry of a nanotube; the electrostatic interactions are reduced due to the large separation of the ‘centre of mass’ of the charges (while still allowing for a significant overlap of the wavefunctions).

3.3. Where exactly are the two dots?

So far we have seen that it is possible to reliably define and control double quantum dots in SWNTs—the question where

precisely the two dots are located, however, has not yet been addressed. As we will point out, from figures 3(a) and (b) it follows that the dots are separated by the centre-gate electrode. We recall that devices A and B are identical except that for device B the centre gate (instead of gate 2) is used to control dot 2. The dashed lines in figures 3(a) and (b) connect triple points corresponding to a constant charge $Q_{1(2)} = \text{const}$, residing on dot 1 (2). A non-zero slope of these lines indicates a cross capacitance, i.e. the gate controlling one of the two dots also affects the chemical potential of the other. A non-zero slope is observed for the $Q_1 = \text{const}$ lines in (b). Hence, the centre gate affects both dots 1 and 2. On the other hand, this is not the case for gate 1 or gate 2 in figures 3(a) and (b). Such behaviour can be explained assuming that the two dots are separated by the centre gate, screening the cross-action of gates 1 and 2. The centre gate, however, located in between the dots and creating a barrier, is not screened and thus acts on the two dots. If the centre gate is capable of creating a tunnel barrier inside the nanotube, so will gates 1 and gate 2 be as well. Also, recall that all the voltages applied to the top gates are within the same range, $V_{\text{Topgate}} \approx 0 \text{ V}$. Consequently, dot 1 is located between gate 1 and the centre gate, whereas dot 2 extends from the centre gate to gate 2. The scenario suggested implies that the part of the SWNT between the gate 1 (2) and the source (drain) electrode has an effectively energy-independent transmission. In fact, this assumption is quite reasonable, taking into account the high quality of Pd–nanotube electrical contacts [19]. Very transparent contacts ($\Gamma \approx \delta E$) lead to a constant, or at least only a slightly modulated transmission. Transport through our device will be dominated by the bottleneck in transmission—the gate-defined double quantum dot.

4. Conclusions

In this paper, we have presented a reliable approach to define and control double quantum dots in SWNTs by using locally

acting top-gate electrodes. That the double quantum dots are not intrinsic to the carbon nanotubes is confirmed by the presented measurements of honeycomb patterns for three different devices. Furthermore, using an electrostatic model, we have been able to characterize the double-dot system quantitatively by extracting its capacitances. Despite these encouraging results, further research is necessary. Challenges to master include the gate control of the quantum-mechanical tunnel coupling of the two quantum dots and the access to regimes of only a few charge carriers per dot. Carbon nanotubes may, due to their unique properties and experimental ease, then play an important role in information technology in future.

Acknowledgments

For theoretical support, we are gratefully indebted to W A Coish and D Loss. We acknowledge the experimental contributions by J Furer, C Hoffmann and J Gobrecht for oxidized Si substrates. Financial support from the Swiss NFS, the NCCR on Nanoscience, EU-FP6-IST-HYSWITCH, and the ‘C und H Dreyfus Stipendium’ (MRG) is greatly appreciated.

References

- [1] Iijima S 1991 *Nature* **354** 56
- [2] Kastner M 1993 *Phys. Today* **46** 24
- [3] Bockrath M, Cobden D H, McEuen P L, Chopra N G, Zettl A, Thess A and Smalley R E 1997 *Science* **275** 1922
- [4] Kouwenhoven L P, Marcus C M, McEuen P L, Tarucha S, Westervelt R M and Wingreen N S 1997 *Proc. Advanced Study Institute on Mesoscopic Electron Transport* ed L L Sohn, L P Kouwenhoven and G Schön (Dordrecht: Kluwer)
- [5] Loss D and DiVincenzo D P 1998 *Phys. Rev. A* **57** 120
- [6] Shnirman A and Schön G 1998 *Phys. Rev. B* **57** 15400
- [7] Burkard G, Loss D and DiVincenzo D P 1999 *Phys. Rev. B* **59** 2070
- [8] Buitelaar M R, Nussbaumer T and Schönenberger C 2002 *Phys. Rev. Lett.* **89** 256801
- [9] Sahoo S, Kontos T, Furer J, Hoffmann C, Gräber M R, Cottet A and Schönenberger C 2005 *Nature Phys.* **1** 99
- [10] Koppens F H L, Folk J A, Elzerman J M, Hanson R, Willems van Beveren L H, Vink I T, Tranitz H P, Wegscheider W, Kouwenhoven L P and Vandersypen L M K 2005 *Science* **309** 1346
- [11] Biercuk M J, Mason N, Martin J, Yacoby A and Marcus C M 2005 *Phys. Rev. Lett.* **94** 026801
- [12] Furer J 2005 *PhD Thesis* University of Basel
- [13] Appenzeller J, Lin Y M, Knoch J and Avouris Ph 2004 *Phys. Rev. Lett.* **93** 196805
- [14] van der Wiel W G, De Franceschi S, Elzermann J M, Fujisawa T, Tarucha S and Kouwenhoven L P 2003 *Rev. Mod. Phys.* **75** 1–22
- [15] Mason N, Biercuk M J and Marcus C M 2004 *Science* **303** 655
- [16] Biercuk M J, Garaj S, Mason N, Chow J M and Marcus C M 2005 *Nano Lett.* **5** 1267
- [17] Sapmaz S, Meyer C, Beliczynski P, Jarillo-Herrero P and Kouwenhoven L P 2006 *Nano Lett.* submitted
- [18] Gräber M R, Coish W A, Hoffmann C, Weiss M, Furer J, Oberholzer S, Loss D and Schönenberger C 2006 *Preprint cond-mat/0603367*
- [19] Javey A, Guo J, Wang Q, Lundstrom M and Dai H 2003 *Nature* **424** 654